

## Optical study of PKS B1322-110, the intra-hour variable radio source

JUAN P. MADRID,<sup>1</sup> ARTEM V. TUNTISOV,<sup>2</sup> MISCHA SCHIRMER,<sup>3</sup> MARK A. WALKER,<sup>2</sup> CARLOS J. DONZELLI,<sup>4</sup>  
KEITH W. BANNISTER,<sup>5</sup> HAYLEY E. BIGNALL,<sup>6</sup> JAMIE STEVENS,<sup>7</sup> CORMAC REYNOLDS,<sup>6</sup> AND SIMON JOHNSTON<sup>5</sup>

<sup>1</sup>*Departamento de Física y Astronomía, La Universidad de Tejas de el Valle del Río Grande, Brownsville, TX 78520, USA*

<sup>2</sup>*Manly Astrophysics, 15/41-42 East Esplanade, Manly, NSW 2095, Australia*

<sup>3</sup>*Max-Planck Institut für Astronomie, Königstuhl 17, D-69117 Heidelberg, Germany*

<sup>4</sup>*Instituto de Astronomía Teórica y Experimental IATE, CONICET - Observatorio Astronómico, Universidad Nacional de Córdoba, Laprida 854, X5000BGR, Córdoba, Argentina*

<sup>5</sup>*CSIRO, Astronomy and Space Science, PO BOX 76, Epping, NSW 1710, Australia*

<sup>6</sup>*CSIRO, Astronomy and Space Science, 26 Dick Perry Avenue, Kensington, WA 6151, Australia*

<sup>7</sup>*CSIRO, Astronomy and Space Science, Paul Wild Observatory, 1828 Yarrie Lake Road, Narrabri, NSW 2390, Australia*

### ABSTRACT

Observations with the Australia Telescope Compact Array revealed intra-hour variations in the radio source PKS B1322-110 (Bignall et al. 2019). As part of an optical follow-up, we obtained Gemini H $\alpha$  and H $\alpha$  continuum (H $\alpha$ C) images of the PKS B1322-110 field. A robust  $19\sigma$  detection of PKS B1322-110 in the H $\alpha$ –H $\alpha$ C image prompted us to obtain the first optical spectrum of PKS B1322-110. With the Gemini spectrum we determine that PKS B1322-110 is a flat-spectrum radio quasar at a redshift of  $z = 3.007 \pm 0.002$ . The apparent flux detected in the H $\alpha$  filter is likely to originate from He II emission redshifted precisely on the Galactic H $\alpha$  narrow-band filter. We set upper limits on the emission measure of the Galactic plasma, for various possible cloud geometries.

*Keywords:* Interstellar medium (847); Radio loud quasars (1349)

### 1. INTRODUCTION

Intra-day variability (IDV) of radio quasars was recognized 30 years ago (Heeschen et al 1987), and became a topic of intense interest a decade later with the discovery of intra-hour variations (IHVs) in PKS 0405-385 by Kedziora-Chudczer et al. (1997). The combination of large amplitude and short timescale seen in that source strongly favoured scintillation as the cause, albeit manifesting in a novel form. Following the discovery of additional IHV sources (J1819+3845 and PKS1257–326; Dennett-Thorpe & de Bruyn 2000; Bignall et al. 2003), IHV was shown to be scintillation due to strongly scattering plasma clouds in the solar neighborhood (Dennett-Thorpe & de Bruyn 2002, 2003; Bignall et al. 2003, 2006).

The rarity of the IHV phenomenon was thus explained by the small probability for a line of sight to intersect such a cloud, and the more common IDV phenomenon is understood as being due to similar, but more distant plasma clouds — with the smaller amplitude and longer timescale of IDV both attributable to the smoothing effect of the radio source size. These studies brought focus

onto the clouds of dense plasma that are responsible for scattering the radio waves: What is their nature? In what physical context do they arise? And how are they energized?

Although it now seems likely that the plasma responsible for IDV and IHV is circumstellar, the material is located at such large distances from the host stars – with impact parameters of order 1 parsec – that stellar winds cannot explain the observed levels of radio-wave scattering (Walker et al. 2017). Thus the nature of the plasma clouds remains a mystery.

To date almost all of the information we have about the scattering plasma has come from studies of radio-wave propagation — either studies of IHV/IDV, or else studies of radio pulsars that seem to be revealing the same population of plasma clouds (Stinebring et al. 2001; Cordes et al. 2006; Walker et al. 2004, 2008; Brisken et al. 2010; Tuntsov et al. 2013). Even during drastic changes in radio flux density, optical observations show constant flux in those sources undergoing IHV/IDVs (e.g. Bannister et al. 2016).

If we could observe the intervening plasma directly, via its own thermal emission, then we could expect some immediate insights to follow from, e.g., density and temperature diagnostics in the emission line ratios, and from the size and morphology of the image of the cloud in any spectral line. These are attractive possibilities, but they

**Table 1.** Observation Log

Program ID	Date	Filter	Grating	Exposure Time (s)
GS-2017A-Q-96	2017 Jun 28	H $\alpha$	None	8500 (10 $\times$ 850)
GS-2017A-Q-96	2017 Jul 01	H $\alpha$ C	None	4250 (5 $\times$ 850)
GS-2018A-FT-106	2018 Apr 09	None	B600	2400 (3 $\times$ 800)
GS-2018A-FT-106	2018 Apr 13	None	R831	800 (1 $\times$ 800)
GS-2018A-FT-106	2018 Apr 20	None	R831	2400 (3 $\times$ 800)

present a substantial observational challenge for the following reasons.

First, the plasma clouds appear to be of small spatial extent, with sizes of some tens of AU suggested by the observed transience of the IHV in J1819+3845 (de Bruyn & Macquart 2015). Second, although the plasma is dense compared to the diffuse ISM, the available estimates of  $n_e \sim 10 - 30 \text{ cm}^{-3}$  (Rickett 2011; Tuntsov et al. 2013) correspond to emission measures  $n_e^2 L \lesssim 0.1 \text{ pc cm}^{-6}$ , if  $L \sim 30 \text{ AU}$  for example, and imply H $\alpha$  intensities  $\lesssim 0.2 \text{ R}$  (Reynolds 2004).<sup>1</sup>

The expected emission measures are at or below the surface brightness limit that was achieved by the Wisconsin H-Alpha Mapper (WHAM) survey of H $\alpha$  emission (Reynolds 2004). WHAM data have relatively low angular resolution (approximately  $1^\circ$ ), whereas we require arcsecond resolution.

Here we report our attempt to detect H $\alpha$  emission from the plasma responsible for the new IHV source PKS B1322–110 using Gemini. Australia Telescope Compact Array observations recently demonstrated that PKS B1322–110 shows intra-day variability in its flux density between 4.3 and 11 GHz (Bignall et al. 2019). PKS B1322–110 is located at an angular distance of  $\sim 8'$  from Spica ( $\alpha$  Virginis), the 16th brightest star in the sky.

## 2. GEMINI OBSERVATIONS AND DATA REDUCTION

### 2.1. Imaging

Observations of PKS B1322-110 were carried out with the Gemini Multiobject Spectrograph (GMOS) in imaging and spectroscopic mode from Gemini South.

Using GMOS, deep H $\alpha$  and H $\alpha$  continuum (H $\alpha$ C) images centered on PKS B1322-110 were obtained. Details are given in Table 1.

The H $\alpha$  filter has its maximum throughput at 6560 Å, the rest-frame wavelength of H $\alpha$  emission. For the H $\alpha$  filter the wavelength interval is 6540–6610 Å (width

at half-maximum). The H $\alpha$ C filter is centered at 6620 Å with a transmission interval of 6590–6650 Å.

The imaging data were obtained on UT 2017 May 28 (H $\alpha$ , cirrus, 0.51 mag transmission variation peak-to-valley) and UT 2017 August 01 (H $\alpha$  continuum, clear sky). On both nights the sky conditions were dark (Gemini SB50 sky brightness quantile). The seeing in the coadded images is 1.14'' (H $\alpha$ ) and 1.22'' (H $\alpha$  continuum).

The data were reduced using the THELI data reduction pipeline (Erben et al. 2005; Schirmer 2013). Standard bias and flat-field correction were applied. The presence of the bright star Spica ( $\alpha$  Virginis,  $V = 0.98$  mag) just  $8'$  north of our target required us to model and subtract the sky background of the individual dithered exposures. This was done following THELI's standard recipes for data processing (Schirmer 2013).

A common astrometric solution was obtained for both filters using SCAMP (Bertin 2006). SCAMP computes astrometric and photometric solutions for any FITS image in an automated way. The individual exposures were registered against the Gaia DR1 astrometric reference catalog. After distortion correction, the images were registered within 1/15th of a pixel with respect to each other. The H $\alpha$  and the H $\alpha$ C images were processed simultaneously omitting their filter information. This allows SCAMP to determine the mean relative throughput difference of the two filters based on stellar magnitudes in the field. The ansatz for our method is that the difference of the two filters should yield a null flux for stars. By following this procedure, the fluxes of the on-band (H $\alpha$ ) and off-band (H $\alpha$ C) images were already calibrated, and deriving their difference image is a straightforward subtraction.

### 2.2. Spectrophotometric calibration

In the absence of observations of a spectrophotometric standard star, a flux calibration of the narrowband images was performed as follows. First, we integrate the effective H $\alpha$  and H $\alpha$  continuum transmission curves including detector quantum efficiency, and find that both narrowband filters transmit a factor 20.3 less than the GMOS  $r$ -band filter. We upscaled the two coadded images by that factor, and compared the  $r$ -band aperture

<sup>1</sup> We measure line intensities in Rayleigh:  $1 \text{ R} = 10^6/4\pi \text{ photons cm}^{-2} \text{ s}^{-1} \text{ sr}^{-1}$ .

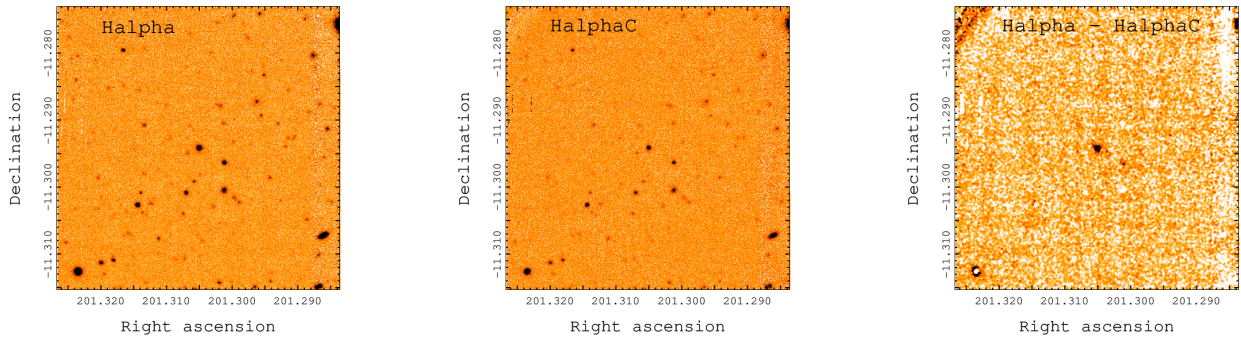


**Figure 1.** Gemini  $H\alpha$  (left) and  $H\alpha C$  (center) images. The subtraction of the  $H\alpha$  continuum from the  $H\alpha$  image ( $H\alpha - H\alpha C$ ) is shown in the right panel. The residual image ( $H\alpha - H\alpha C$ ) has been smoothed with a Gaussian kernel of five pixels for display purposes. All images are centered on PKS B1322-110, and show an area of  $150 \times 150$  arcseconds. PKS B1322-110 is the only source that shows a clear excess of  $H\alpha$  flux on the section of the residual image shown above.

magnitudes in these images with the PanSTARRS-DR1  $r$  magnitudes of the same field.

### 2.3. Spectroscopy

GMOS spectra of PKS B1322-110 were obtained with two gratings: B600 and R831. The B600 grating has a blaze wavelength of  $4610 \text{ \AA}$ . Likewise, the R831 grating has a blaze wavelength of  $7570 \text{ \AA}$ . This observing configuration is adopted in order to have a wide spectral coverage with a high signal-to-noise from  $\sim 3500$  to  $\sim 8000 \text{ \AA}$ , as shown in the final spectrum in Figure 2.

Spectroscopic data were reduced by applying a sequence of standard PYRAF tasks available through the Gemini package. The data reduction procedure used here has been described in detail in Madrid & Donzelli (2013). The spectra of the spectrophotometric standard star EG274 are used to flux calibrate the science spectra.

## 3. RESULTS

The narrowband images,  $H\alpha$  and  $H\alpha$  continuum, are presented in Figure 1. The  $H\alpha$  narrowband filter is centered on the rest-frame wavelength of  $H\alpha$  ( $6560 \text{ \AA}$ ). The  $H\alpha$  continuum filter is adjacent to the  $H\alpha$  filter and it is designed to allow for the removal of the underlying continuum. By obtaining images with these two filters and computing their difference ( $H\alpha - H\alpha C$ ) one can detect sources with excess  $H\alpha$  emission.

Both the  $H\alpha$  and  $H\alpha$  continuum images show dozens of sources in the field, most of these sources are galaxies or stars; see Fig. 1. On the other hand, the difference image ( $H\alpha - H\alpha C$ ) has only one clear source on the entire central part of the frame, also shown in Fig. 1.

The clear detection of excess flux in the  $H\alpha$  filter ( $19 \sigma$ ) coincident with PKS B1322-110 was compelling and prompted us to request additional time on Gemini South in order to obtain a spectrum of PKS B1322-110.

Also, until now, the nature and redshift of PKS B1322-110 have remained unknown.

The calibrated GMOS spectrum of PKS B1322-110 obtained during the spectroscopic campaign is presented in Fig. 2. This spectrum shows a prominent  $Ly\alpha$  line and the associated  $Ly\alpha$  forest. The  $Ly\beta$  and C IV emission lines are also prominent. Using the above emission lines, jointly with other prominent lines like O I, and N V we determine that the redshift of PKS B1322-110 is  $z = 3.007 \pm 0.002$ . The optical spectrum of PKS B1322-110 is characteristic of a quasar; see for instance the composite quasar spectra templates from the SDSS (Vanden Berk et al. 2001). Considering its radio properties (Griffith et al. 1994) PKS B1322-110 can be classified as a flat spectrum radio quasar (FSRQ).

Given that the redshift of PKS B1322-110 is now determined to be  $z=3.007$  the presence of an excess flux at  $6560 \text{ \AA}$ , the rest-frame wavelength of  $H\alpha$ , is likely due to the redshifted emission of the He II line. He II is an emission line with a rest-frame wavelength of  $1640 \text{ \AA}$  that is commonly found on quasar spectra (e.g. Wilkes 1986; Jacobsen et al. 2003). The observed emission of the He II line at the redshift of PKS B1322-110 is  $\lambda_{obs} = 1640 \times (1 + z) = 6560 \text{ \AA}$ , falling exactly on the passband of the Galactic  $H\alpha$  narrowband filter.

At a redshift of  $z=3.007$ , PKS B1322-110 is at the high end of the redshift distribution of scintillating radio sources. Indeed, Lovell et al. (2008) found that radio sources that show interstellar scintillation drop steeply beyond redshift  $\sim 2$ .

## 4. LINE EMISSION CONSTRAINTS

### 4.1. An upper limit for the $H\alpha$ flux

The Gemini spectrum of PKS 1322-110, displayed in Figures 2 and 3, lacks any conspicuous narrow line emission at the wavelength of Galactic  $H\alpha$ , where emission from the plasma responsible for radio scintillations might be expected. Using the Gemini spectrum we

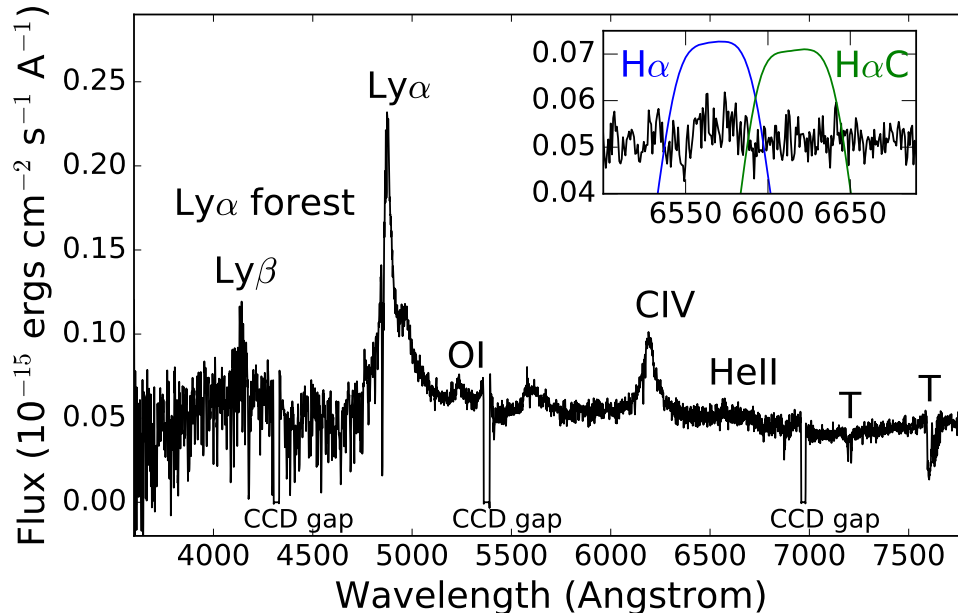


**Figure 2.** GMOS spectrum of PKS B1322-110. This spectrum shows the combined, calibrated data obtained with both gratings, i.e. B600 and R831. The letter T denotes prominent telluric absorption lines that are present, as expected, at wavelengths larger than 6700 Å. The inset zooms on the section of the spectrum at the wavelength of Galactic H $\alpha$ . In this inset, the transmission curves for the H $\alpha$  (blue line) and H $\alpha$  continuum (green line) filters are overplotted. At the redshift of  $z=3.0$  the He II line falls precisely in the passband of the Galactic H $\alpha$  filter. The spectrum is displayed at the observed wavelength.

derive an upper limit for the H $\alpha$  flux hypothetically emanating from the intervening plasma that might be blended with the active galactic nucleus (AGN). These upper limits are derived by measuring the variation in the spectrum from one resolution element to the next. The resolution element corresponds to three pixels, that is, 2.2Å or 102 km s $^{-1}$  at the H $\alpha$  wavelength (approximately 6563Å in air). The standard deviation of the spectrum is  $\approx 3.4 \times 10^{-18}$  erg cm $^{-2}$  s $^{-1}$  Å $^{-1}$ . This value is measured within 10 Å to either side of H $\alpha$  in the spectrum running-averaged to the resolution of 2.2 Å. Integrating over the line, we conclude that the  $3\sigma$  upper limit to the H $\alpha$  flux of plasma that might be blended with the AGN is  $2.3 \times 10^{-17}$  erg cm $^{-2}$  s $^{-1}$ .

We note that the value of the standard deviation given above is larger than our estimate of the noise in the spectrum, which is  $\approx 1.5 \times 10^{-18}$  erg cm $^{-2}$  s $^{-1}$  Å $^{-1}$ . This difference presumably reflects intrinsic structure in the AGN spectrum.

#### 4.2. Spatial extent of the intervening plasma

The limit on the emission measure of the plasma depends on its assumed spatial extent. As the scintillations of PKS B1322-110 have been sustained for at least 2 years (Bignall et al. 2019), the proper motion of the scattering plasma sets a lower limit on the size of the cloud responsible for the scintillations. Assuming the plasma is comoving with Spica – which is consistent with the measured annual cycle of PKS B1322-110 (Bignall

et al. 2019) – this lower limit is  $\approx 100$  milliarcseconds (mas) in one direction on the sky.

In the case of a the plasma cloud that is at least 100 mas by 100 mas its brightness upper limit is 410 R. To convert brightness to emission measure we assume Case B recombination at  $T = 10^4$  K, giving a conversion factor of 0.361 R cm $^6$  pc $^{-1}$  (Table 14.2 of Draine et al. 2011). The emission measure upper limit is then  $1.1 \times 10^3$  cm $^{-6}$  pc.

The foregoing calculation applies to a compact plasma cloud whose emission is blended with that of the background quasar. We searched for extended emission by modeling the long-slit data obtained by Gemini as a sum of a compact source (convolved with a PSF along the slit) and a sky background that is flat along the slit. We remove the model from the observed data and analyze the residual. No extended emission can be seen at the wavelength of H $\alpha$  down to the level  $\sim 1.9 \times 10^{-17}$  erg cm $^{-2}$  s $^{-1}$  Å $^{-1}$  arcsec $^{-2}$ . For emission wider than the slit this corresponds to the intensity density  $3\sigma$  limit of 10 R Å $^{-1}$ ; integrating over the spectral resolution element, one obtains the intensity limit of 22 R equivalent to EM  $\approx 62$  cm $^{-6}$  pc under the stated equilibrium conditions. This estimate assumes a unit surface filling fraction maintained on arcsecond spatial scales.

A third scenario for the spatial extent of the intervening plasma is that it is uniform and extended over the entire length of the slit. In this case, any plasma



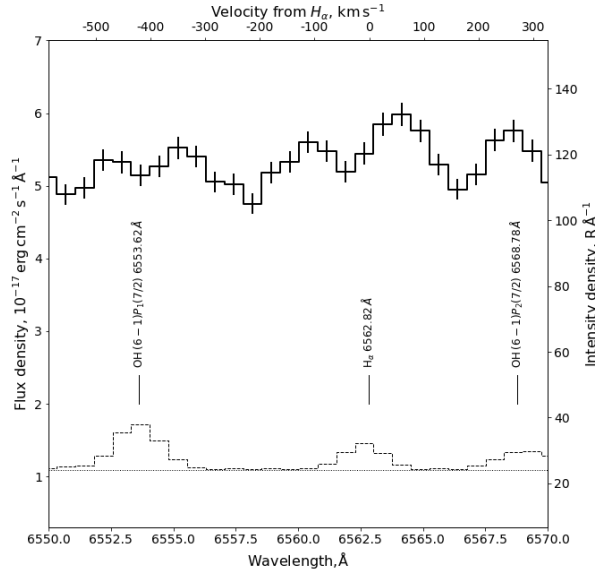


**Figure 3.** Zoom-in of the AGN (solid) and sky background (dashed) spectra of PKS 1322–110 within  $20\text{\AA}$  adjacent to the Galactic  $H\alpha$  position; the horizontal dotted line shows our estimate of the sky continuum level. Line identifications are given for the night sky background, based on [Osterbrock et al. \(1996\)](#) and [Hanuschik \(2003\)](#).

emission would have been subtracted with the sky modeling and could not be seen in the residuals. The sky spectrum does display a line at the wavelength of  $H\alpha$ , which integrates to  $17\text{ R}$  above the estimated continuum level of  $24\text{ R}\text{\AA}^{-1}$ . At the spectral resolution of  $\sim 2\text{\AA}$

we cannot distinguish Galactic  $H\alpha$  emission from that of the night sky and therefore can only set an upper limit on the intensity of the intervening plasma emission at  $17\text{ R}$ , which corresponds to the emission measure of  $47\text{ cm}^{-6}\text{ pc}$  – again assuming a unit surface filling fraction, this time sustained over a scale of a few arcminutes.

## 5. CONCLUSION

Gemini narrowband imaging resulted in an apparent  $H\alpha$  detection toward the fast scintillator PKS B1322–110, and we therefore undertook follow-up spectroscopy with Gemini. The spectroscopy demonstrated that Galactic  $H\alpha$  emission was not responsible for the signal that we observed in our images. In part the signal we observed in our imaging data is due to  $\text{He II}$  emission in the quasar redshifted to the wavelength of Galactic  $H\alpha$ . We have determined limits on the possible  $H\alpha$  surface brightness of the intervening Galactic plasma cloud, depending on its size. However, even in the case of a very extended cloud the corresponding limits on emission measure are well above the values expected from modeling the scintillations of other radio sources.

We thank Nathan Pope (CSIRO) for his help with computing resources. Based on observations obtained at the Gemini Observatory which is operated by AURA under a cooperative agreement with the NSF on behalf of the Gemini partnership: the National Science Foundation (United States), the National Research Council (Canada), CONICYT (Chile), Ministério da Ciência, Tecnologia e Inovação (Brazil) and Ministerio de Ciencia, Tecnología e Innovación Productiva (Argentina).

## REFERENCES

- Bannister, K. W., Stevens, J., Tuntsov, A. V., et al., 2016, *Science*, 351, 354
- Bertin, E. 2006, *Astronomical Data Analysis Software and Systems XV ASP Conference Series*, Vol. 351, 112
- Bignall, H. E., Jauncey, D., L., et al., 2003, *ApJ*, 585, 653
- Bignall H. E., Macquart J.-P., Jauncey D. L., et al., 2006, *ApJ*, 652, 1050
- Bignall, H. E., Reynolds, C.R., Stevens, J., et al., 2019, *MNRAS*, 487, 4372
- Briskin, W. F., Macquart, J.-P., Gao, J. J., et al, 2010, *ApJ*, 708, 232
- Cordes, J. M., Rickett, B. J., Stinebring, D. R., Coles, W. A. 2006, *ApJ*, 637, 346
- de Bruyn, A. G., Macquart, J.-P., 2015, *A&A*, 574, 125
- Dennett-Thorpe J. & de Bruyn A. G., 2000, *ApJL*, 529, L65
- Dennett-Thorpe J. & de Bruyn A. G., 2002, *Nature*, 415, 57
- Dennett-Thorpe, J. & de Bruyn, A.G., 2003, *A&A*, 404, 113
- Draine, B. T. 2011, *Physics of the Interstellar and Intergalactic Medium*, Princeton University Press
- Erben, T., Schirmer, M., Dietrich, J. P. 2005, *AN*, 326, 432
- Griffith, M. R., Wright, A. E., Burke, B. F., Ekers, R. D. 1994, *ApJS*, 90, 179
- Hanuschik R. W., 2003, *A&A*, 407, 1157
- Heeschen, D.S., Krichbaum, T., Schalinsky, C.J., Witzel, A., 1987, *AJ*, 94, 1493
- Jakobsen, P., Jansen, R. A., Wagner, S., et al., 2003, *A&A*, 397, 891
- Kedziora-Chudczer L., Jauncey D. L., Wieringa M. H., et al., 1997, *ApJL*, 490, L9
- Lovell, J. E. J., Rickett, B. J., Macquart, J.-P., Jauncey, D. L., et al., 2008, *ApJ*, 689, 108
- Madrid, J. P. & Donzelli, C. J. 2013, *ApJ*, 710, 158
- Osterbrock D. E., Fulbright J. P., Martel A. R., et al., 1996, *PASP*, 108, 277

- Reynolds, R. J. 2004, *AdSpR*, 34, 27
- Rickett, B. J., 2011, *AIP Conf. Ser. Vol. 1366*, 107
- Schirmer, M. 2013, *ApJSS*, 209, 21
- Stinebring, D. R., McLaughlin, M. A., Cordes, J. M., et al. 2001, *ApJL*, 549, L97
- Tuntsov, A. V., Bignall, H. E., Walker, M. A. 2013, *MNRAS*, 429, 2562
- Vanden Berk, D. E., Richards, G. T., Bauer, A., et al. 2001, *AJ*, 122, 549
- Walker, M. A., Melrose, D. B., Stinebring, D.R., Zhang, C.M., 2004, *MNRAS*, 354, 43
- Walker, M. A., Koopmans, L. V. E., Stinebring, D.R., van Straten, W., 2008, *MNRAS*, 388, 1214
- Walker, M. A., Tuntsov, A. V., Bignall, H. E. et al., 2017, *ApJ*, 843, 15
- Wilkes, B. 1986, *MNRAS*, 218, 331